Int J Earth Sci (Geol Rundsch) (2002) 91:1005–1016
DOI 10.1007/s00531-002-0281-z

ORIGINAL PAPER

Ulrich Lange · Michael Bröcker · Klaus Mezger
Jerzy Don

Geochemistry and Rb–Sr geochronology of a ductile shear zone in the Orlica-Śnieżnik dome (West Sudetes, Poland)

Received: 12 August 2001 / Accepted: 29 April 2002 / Published online: 26 June 2002

Abstract Amphibolite-facies orthogneisses of the Orlica-Śnieżnik dome in the West Sudetes (Poland) show a local continuous transition from weakly deformed augen gneisses to finely laminated mylonites. Field evidence indicates that ductile shearing developed pre- or syntectonically to a migmatization event. Bulk-rock compositions of variably deformed samples yield no indications for deformation- and/or fluid-enhanced element mobility and redistribution. ^{87}Rb–^{86}Sr geochronology (biotite, phengite, whole rock) places time constraints on the deformation process and the post-orogenic cooling history. Phengite– and biotite–whole-rock pairs yield Rb–Sr ages of 340 to 334 Ma and 335 to 294 Ma, respectively, independent of the degree of deformation. The weighted mean of phengite–whole-rock pairs indicates an age of 337.4±2.3 Ma. Combining most of the biotite–whole-rock data yields a weighted mean age of 328.6±4.4 Ma. Because of their different closure temperatures for the Rb–Sr system, these differences are interpreted to date cooling after a thermal event. Direct dating of the deformation is not possible, but the cooling history record defines a minimum age for the development of ductile shearing and the last migmatization event. These time constraints provide evidence for the initiation of crustal collapse during or immediately following peak metamorphic conditions. The results of this study further document the importance of Variscan metamorphism in the Orlica-Śnieżnik dome.

Keywords Ductile deformation · Orlica-Śnieżnik dome · Rb–Sr geochronology · Variscan metamorphism

U. Lange (✉) · M. Bröcker · K. Mezger
Institut für Mineralogie, Universität Münster, Corrensstr. 24, Münster, Germany
e-mail: langeul@nwz.uni-muenster.de

J. Don
Instytut Nauk Geologicznych, Uniwersytet Wrocławski, ul. Cybulskiego 30, 50-205 Wrocław, Poland

Introduction

Geochronological information on the timing of deformation processes provides important constraints for the interpretation of metamorphic P–T–t-deformation paths. The most promising tools to determine deformation ages are $^{40}Ar/^{39}Ar$ and Rb–Sr geochronology of potassic white mica and U–Pb dating of titanite (e.g. Gromet 1991; Getty and Gromet 1992; Scheuber et al. 1995; Freeman et al. 1997, 1998a, 1998b; Fossen and Dallmeyer 1998). However, with these methods direct dating of deformation is only possible if the studied phase formed or recrystallized at or below the closure temperature for the specific mineral and isotope system. If crystallization or recrystallization occurred at a higher temperature, cooling ages will be obtained that provide a lower time limit for the deformation event.

This paper presents the first results of a detailed study of the isotope geochemistry and geochronology of the Orlica-Śnieżnik dome at the north-eastern margin of the Bohemian Massif (West Sudetes, Poland; Fig. 1). The contribution focuses on variably deformed orthogneisses ('Śnieżnik gneisses') that have undergone upper amphibolite-facies metamorphism and ductile deformation (e.g. Don et al. 1990). On outcrop-scale these rocks show locally a continuous transition from weakly deformed augen gneisses to finely laminated mylonites. The shear zones are not tectonic boundaries between different crustal segments, but developed within apparently homogeneous orthogneisses. Field evidence indicates that ductile shearing developed pre- or syntectonically to a migmatization event. Thus, direct dating of the deformation is not possible by application of the Rb–Sr method. The complex P–T–t-deformation path of the orthogneisses is not well understood. Critical parameters for further interpretation are the timing of the deformation process and the chronology of the post-peak metamorphic cooling history. In this study, these topics are addressed using Rb–Sr dating of mica–whole-rock pairs.

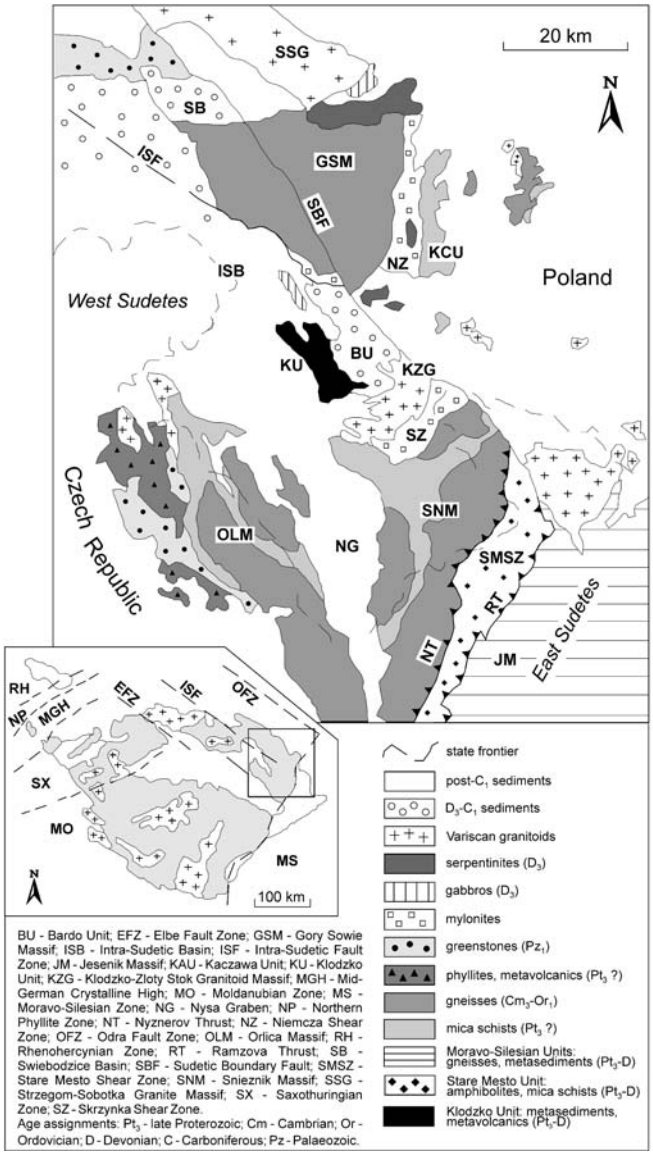

Fig. 1 Geological sketch map of the West Sudetes with an *inset map* of the central European Variscides (modified after Mazur and Aleksandrowski 2001)

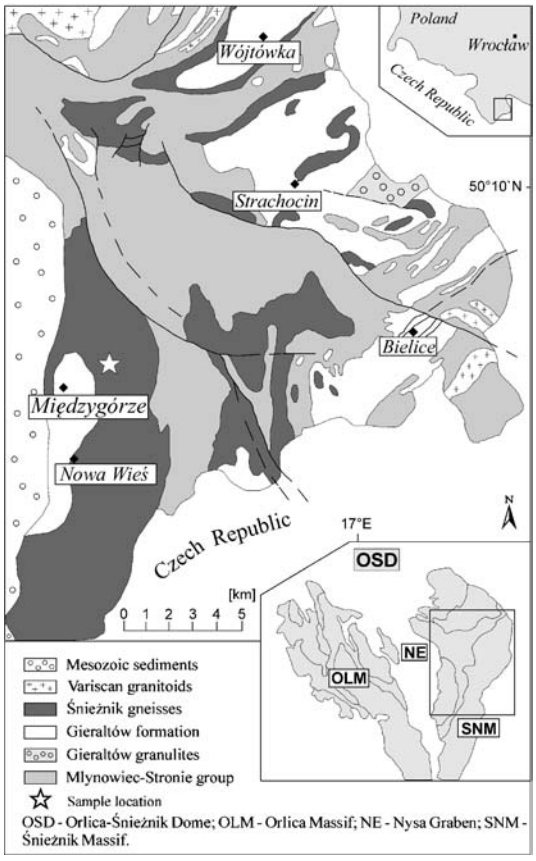

Fig. 2 Geological sketch map of the eastern part of the Orlica-Śnieżnik dome (OSD) with an inset map of the Orlica-Śnieżnik dome (modified after Dumicz 1979)

Geological background

The Orlica-Śnieżnik dome represents the easternmost unit of the West Sudetes (Figs. 1 and 2), and is bordered by two NW-trending fault zones: the Sudetes Marginal fault in the north-east and the Busin Fault in the south-west. Both fault zones extend parallel to the Odra and Elbe Fracture Zones, the major lineaments dividing the West Sudetes from other crustal segments within the Variscides. The Orlica-Śnieżnik dome is cut by the Cretaceous Nysa graben and divided into the eastern Lądek-Śnieżnik metamorphic massif and the western Góry Bystrzyckie and Góry Orlickie Mts. (Don et al. 1990). The tectono-metamorphic evolution of the study area is complex and no generally accepted geodynamic interpretation could be established. Only a short outline of the local geology is given here. For a comprehensive description of this complex tectono-stratigraphic domain see Don et al. (1990, and references therein).

The Orlica-Śnieżnik dome (Figs. 1 and 2) is mainly composed of amphibolite-facies orthogneisses that are associated with metasediments and minor metavolcanic rocks (e.g. Don et al. 1990). Three major lithological units were distinguished (Don et al. 1990). (1) The Młynowiec–Stronie group, which comprises plagioclase gneisses with minor mica schists (Młynowiec formation, >2,000 m thick). This sequence is overlain by a variegated succession of biotite- to staurolite-grade mica schists, paragneisses, quartzites, marbles and amphibolites (Stronie formation, ca. 3,000 m thick). (2) The variably deformed amphibolite-facies Śnieżnik orthogneisses. (3) The Gierałtów formation, which is dominated by partly migmatitic two-feldspar orthogneisses; minor eclogite and granulite blocks and lenses are enclosed in the Gierałtów gneisses.

It is not known whether Śnieżnik and Gierałtów gneisses, differing in textures and some bulk-compositional features, are derived from a single igneous suite or represent genetically unrelated intrusive rock series (e.g. Turniak et al. 2000). Protolith ages for both types are broadly con-

strained between 500 and 400 Ma (Śnieżnik gneisses: 487±11 Ma, Rb–Sr whole-rock isochron, van Breemen et al. 1982; 395±35 Ma, Rb–Sr whole-rock isochron, Borkowska et al. 1990; 503±4 Ma, 488 +4/–7 Ma, U–Pb single zircon ages, Oliver et al. 1993; 540 to 500 Ma, ^{207}Pb–^{206}Pb ages based on U–Pb single zircon dating, Borkowska and Dörr 1998; 540 to 500 Ma, ^{207}Pb-^{206}Pb ages based on U–Pb single zircon dating, Borkowska and Orlowski 1999; 495±7 Ma, U–Pb SHRIMP dating, Turniak et al. 2000; Gierałtów gneisses: 464±18 Ma, Rb–Sr whole-rock isochron, Borkowska et al. 1990; 495±14 Ma, U–Pb SHRIMP dating, Turniak et al. 2000; series of granitoid orthogneisses in the West Sudetes (from the Izera Mountains in the NW to the Orlica-Śnieżnik dome in the SE): 515 to 502 Ma, single zircon dating (evaporation and vapour transfer method), Kröner et al. 2001).

The available geochronological database for the metamorphism in the Orlica-Śnieżnik dome is small, indicating late Devonian to Carboniferous ages, mostly in the range from 350 to 330 Ma (Śnieżnik gneisses: 335±5 Ma, Rb–Sr whole-rock–biotite dating, Borkowska et al. 1990; eclogites associated with the Gierałtów gneisses: 341±7, 337±4, 329±6, 352±4 Ma, Sm–Nd garnet–pyroxene–whole-rock dating, Brueckner et al. 1991; gneisses associated with the eclogites: 338.4±4.5 to 328±2 Ma, ^{40}Ar/^{39}Ar ages for biotite, muscovite and hornblende, Steltenpohl et al. 1993). A few data indicate earlier metamorphic events (Gierałtów gneisses: 382±16 Ma, K–Ar biotite dating, Bakun-Czubarow 1968; mafic granulites: 369±1 to 360±6 Ma, ^{207}Pb–^{206}Pb zircon ages based on U–Pb multigrain dating, Klemd and Bröcker 1999). Unsolved problems include the significance of pre-Variscan metamorphism and the temporal and structural relationships between orthogneisses and eclogites or granulites. Application of different geochronological methods that cover a large range of closure temperatures yielded a suspicious conformity in ages. For example, Sm–Nd dating of eclogites (garnet, omphacite, whole rock) and ^{40}Ar/^{39}Ar phengite chronology of amphibolite-facies gneisses provided overlapping ages between 341 and 328 Ma (Brueckner et al. 1991; Steltenpohl et al. 1993; Klemd and Bröcker 1999).

P–T conditions are only well constrained for eclogites and granulites. For these rocks, estimated peak pressures lie in the coesite stability field with pressures in excess of 27 kbar at temperatures of 700–800 °C (for eclogites) and 800–1,000 °C (for granulites; Bakun-Czubarow 1991a, 1991b; Klemd et al. 1995; Bröcker and Klemd 1996; Kryza et al. 1996; Klemd and Bröcker 1999). The peak-pressure conditions for the Gierałtów gneisses reached eclogite-facies conditions (Bröcker and Klemd 1996). The high-pressure metamorphism recorded in eclogites and granulites is interpreted by many workers as an in-situ process (e.g. Smulikowski 1967; Brueckner et al. 1991; Bröcker and Klemd 1996). In contrast, Don (1989) considered the eclogites to be exotic tectonic inclusions within gneisses. The Śnieżnik and Gierałtów orthogneisses are not well suited for petrological investigations because mineral assemblages particularly appropriate for a rigorous phase petrological analysis or for application of geothermobarometers are absent. At least upper amphibolite-facies temperatures are indicated for both types by variable degrees of migmatization.

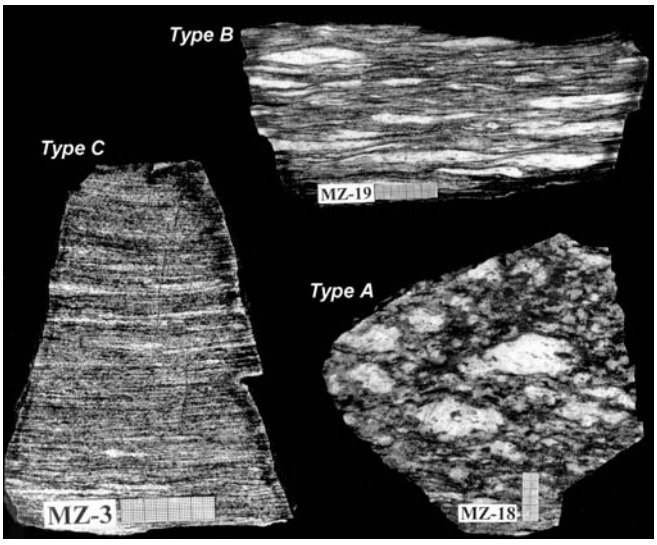

Fig. 3 Granitoid orthogneisses from the Międzygórze area representing progressive increase of deformation; *type A* augen gneiss, *type B* laminated augen gneiss and *type C* mylonitic gneiss

The timing of distinct stages in the deformation history of the Śnieżnik and Gierałtów gneisses is currently not known with certainty. The polyphase structural evolution involves at least three, possibly up to seven stages (e.g. Dumicz in Don et al. 1990). Some workers interpret the main deformation (D_2 and D_3) as a Late Caledonian process, whereas others emphasize the importance of Early to Late Carboniferous events (for a discussion of this controversial issue see, e.g. Don et al. 1990, Cymerman et al. 1997; Kröner et al. 2001). Field observations indicate that the granitic precursors of the Śnieżnik gneisses intruded the Młynowiec-Stronie group and suggest an emplacement pre- or syntectonically to the D_2 event, but after the D_1 phase recognized within the country rocks (Don et al. 1990). According to Don (1982a, 1982b), the Śnieżnik granites underwent dynamic transformation into mylonitic Śnieżnik augen gneisses during the D_2 stage. In contrast, Żelaźniewicz (personal communication) interpreted the progressive shearing of the Śnieżnik gneisses as a D_3 feature. For detailed structural interpretations see Dumicz (1979, 1988), Don (1977, 1982a, 1982b), Żelaźniewicz (1984, 1988), Don et al. (1990), Prikryl et al. (1996) and Cymerman et al. (1997).

Sample description

All samples were collected near Międzygórze (Fig. 2), at the location that is called ‘The Tower’ outcrop (Don 2001). The outcrop is located on the northern flank of the Bogoryja valley, about 250 m after the last house of the village, where variably deformed orthogneisses (Fig. 3) show the continuous transition from weakly de-

Table 1 Selected electron microprobe analyses of phengites from granitoid orthogneisses collected near Międzygórze. Oxides are given in wt%. Cations are calculated on the basis of 22 oxygens. H_2O based on stoichiometry

Type[a]	A	A	A	A	A	B	B	B	B	B	C	C	C	C	C
Sample	7	7	10	18	18	22	22	22	22	22	3	3	3	20	20
Spot	F5	D3	H5	E8	F10	C6	C9	D10	E4	E10	A7	A8	C7	A4	D3
SiO_2	48.94	48.36	47.15	49.96	47.84	50.26	49.17	47.14	47.30	48.79	48.35	47.77	50.14	49.36	49.06
TiO_2	0.47	0.34	0.45	1.51	0.64	1.00	0.86	0.54	0.59	0.48	0.47	0.59	0.40	0.57	0.57
Al_2O_3	29.13	30.69	32.54	26.98	30.63	27.06	28.24	32.47	31.41	29.19	29.41	31.19	28.04	28.63	30.02
Cr_2O_3	0.02	0.01	0.01	0.08	0.01	0.00	0.05	0.03	0.05	0.01	0.04	0.02	0.08	0.00	0.01
MgO	2.33	1.95	1.48	2.67	1.97	2.68	2.51	1.40	1.76	2.24	2.25	1.72	2.47	2.30	2.04
CaO	0.00	0.00	0.01	0.00	0.00	0.00	0.00	0.01	0.01	0.03	0.00	0.00	0.00	0.00	0.02
MnO	0.03	0.09	0.03	0.01	0.06	0.01	0.09	0.08	0.00	0.04	0.05	0.00	0.05	0.07	0.08
FeO	3.48	2.90	2.71	3.22	3.39	3.29	3.64	2.66	3.03	3.29	3.68	2.99	3.49	3.60	3.01
BaO	0.05	0.05	0.05	0.10	0.15	0.10	0.11	0.07	0.07	0.09	0.09	0.07	0.22	0.22	0.24
Na_2O	0.23	0.22	0.28	0.16	0.23	0.24	0.16	0.28	0.28	0.16	0.19	0.33	0.19	0.19	0.26
K_2O	10.97	10.72	10.84	10.74	10.82	10.84	10.77	10.69	10.82	10.69	10.71	10.83	10.58	10.77	10.36
H_2O	4.46	4.47	4.48	4.46	4.46	4.47	4.46	4.47	4.46	4.45	4.44	4.47	4.48	4.47	4.49
Total	100.09	99.79	100.03	99.89	100.19	99.94	100.04	99.83	99.76	99.43	99.67	99.97	100.14	100.17	100.15
Si	6.575	6.489	6.320	6.713	6.425	6.750	6.615	6.323	6.367	6.583	6.527	6.411	6.718	6.630	6.550
Ti	0.047	0.034	0.050	0.152	0.065	0.101	0.087	0.054	0.060	0.049	0.048	0.059	0.040	0.060	0.060
Al	4.613	4.853	5.138	4.274	4.849	4.283	4.478	5.133	4.983	4.641	4.679	4.935	4.427	4.531	4.727
Cr	0.002	0.001	0.001	0.009	0.001	0.000	0.005	0.003	0.005	0.001	0.004	0.002	0.008	0.000	0.001
Mg	0.467	0.389	0.295	0.536	0.393	0.536	0.503	0.280	0.354	0.450	0.453	0.343	0.494	0.460	0.407
Ca	0.000	0.000	0.001	0.000	0.000	0.000	0.000	0.001	0.001	0.004	0.000	0.000	0.000	0.000	0.003
Mn	0.003	0.010	0.000	0.001	0.007	0.002	0.010	0.009	0.000	0.004	0.005	0.000	0.005	0.010	0.010
Fe	0.391	0.325	0.300	0.362	0.380	0.370	0.410	0.298	0.342	0.372	0.415	0.336	0.391	0.400	0.340
Ba	0.003	0.003	0.000	0.005	0.008	0.005	0.006	0.003	0.004	0.005	0.005	0.004	0.012	0.010	0.010
Na	0.060	0.057	0.070	0.040	0.060	0.062	0.041	0.074	0.072	0.042	0.050	0.085	0.050	0.050	0.070
K	1.880	1.835	1.850	1.841	1.853	1.857	1.849	1.829	1.858	1.839	1.844	1.854	1.808	1.840	1.770
Total	14.040	13.996	14.032	13.933	14.042	13.966	14.002	14.007	14.044	13.988	14.031	14.030	13.953	13.996	13.940

[a] Augen gneiss (type A), laminated augen gneiss (type B), mylonitic gneiss (type C)

formed augen gneiss (type A), to laminated augen gneiss (type B) and finely banded, mylonitic rocks (type C). Individual shear zones within this heterogeneously deformed rock volume range in width from a few centimetres to about 2.5 m and can only be traced for short distances in the outcrop locality. Across strike the transition from augen gneisses into mylonitized granitoids is observed over distances of tens of centimetres. The mineral assemblage of all investigated gneisses is dominated by alkali feldspar, plagioclase, quartz, biotite and white mica. As additional constituents, garnet, titanite, epidote/clinozoisite, zircon, apatite and opaques occur in minor amounts. Variable degrees of retrogression are indicated by weak chloritization of biotite and sericitization of feldspars. The least deformed textural variant (type A; Fig. 3) is characterized by large subhedral K-feldspar augen (up to 7 cm). Progressively increasing strain produced a laminated augen gneiss (type B; Fig. 3) with strongly flattened K-feldspar porphyroclasts (individual laminae 2–10 mm thick). As observed in type A, larger quartz grains show a core-and-mantle structure. Further deformation produced a mylonitic gneiss (type C; Fig. 3) with homogeneous banding of polymineralic felsic and mafic layers. The dynamic fabric is partially overprinted by features of a post-deformational static high-temperature recrystallization that produced an almost equigranular fabric within individual layers. Similar textures were reported from orthogneisses in the Bystrzyca Mts (western part of Orlica-Śnieżnik dome), where Żelaźniewicz (1984) recognized that the main metamorphism was largely a post-tectonic process that caused a static high-temperature recrystallization. Modal proportions of the main constituents have not been changed significantly during transformation from type A to type C.

Superimposed on the mylonitic fabric, small amounts of migmatites developed locally within gneisses of type C. In this case, the foliation is replaced by nebulitic textures without an internal deformation fabric, indicating that the migmatization was a late syn- or a post-kinematic process. Because of specific outcrop characteristics, it was not possible to collect samples from migmatized rocks.

Analytical methods

The chemistry of phengite and biotite mineral compositions were determined with a SX-50 CAMECA microprobe at the Mineralogisches Institut der Universität Würzburg. Operating conditions were a 15-kV acceleration voltage, a 15-nA beam current, a spot diameter of 5 μm and a counting time of 20–30 s. Natural and synthetic minerals were used for standardization. The raw data were corrected with a ZAF procedure using the PAP software provided by Cameca. Selected electron microprobe analyses are reported in Tables 1 and 2.

Table 2 Selected electron microprobe analyses of biotites from granitoid rocks collected near Międzygórze. Oxides are given in wt%. Cations are calculated on the basis of 22 oxygens. H_2O based on stoichiometry

Type[a]	A	A	A	A	A	B	B	B	B	B	C	C	C	C	C
Sample	7	7	10	18	18	22	22	22	22	22	3	3	3	20	20
Spot	G3	F4	L2	E7	D2	C3	E6	B2	B8	A10	E1	E10	G9	C11	G1
SiO_2	35.72	35.71	34.91	35.01	36.85	35.73	36.54	35.44	35.40	34.47	35.95	35.74	35.44	35.44	35.72
TiO_2	2.50	3.44	2.57	3.21	3.26	3.12	3.72	3.80	3.19	3.16	3.38	3.26	2.85	3.13	3.08
Al_2O_3	17.62	16.96	18.12	17.23	16.78	17.17	16.71	16.24	17.24	17.80	16.86	17.17	17.49	16.82	18.46
Cr_2O_3	0.06	0.02	0.02	0.07	0.00	0.00	0.02	0.05	0.02	0.00	0.03	0.00	0.01	0.05	0.03
MgO	7.77	7.24	6.95	7.47	7.54	7.64	7.62	7.17	6.89	5.67	7.17	7.38	7.24	7.26	6.48
CaO	0.00	0.00	0.02	0.03	0.00	0.00	0.00	0.00	0.00	0.03	0.02	0.00	0.01	0.00	0.05
MnO	0.23	0.30	0.34	0.27	0.15	0.25	0.19	0.27	0.33	0.34	0.24	0.21	0.18	0.24	0.21
FeO	21.99	22.63	23.35	23.81	21.75	22.60	21.49	22.84	23.21	25.51	23.15	23.19	23.10	23.16	22.69
BaO	0.00	0.00	0.00	0.00	0.00	0.00	0.00	0.00	0.00	0.00	0.00	0.00	0.00	0.00	0.00
Na_2O	0.13	0.09	0.07	0.08	0.08	0.14	0.09	0.06	0.12	0.06	0.09	0.13	0.05	0.02	0.18
K_2O	9.31	9.49	9.46	8.87	9.47	9.32	9.49	9.27	9.40	9.38	9.29	9.29	9.13	9.47	9.08
H_2O	3.89	3.89	3.87	3.88	3.92	3.90	3.92	3.85	3.88	3.85	3.90	3.91	3.88	3.87	3.91
Total	99.22	99.78	99.67	99.93	99.80	99.88	99.80	98.99	99.69	100.28	100.09	100.28	99.37	99.45	99.89
Si	5.508	5.505	5.410	5.408	5.632	5.494	5.588	5.516	5.477	5.366	5.526	5.485	5.481	5.500	5.470
Ti	0.290	0.399	0.300	0.372	0.375	0.360	0.428	0.445	0.372	0.370	0.391	0.376	0.331	0.370	0.350
Al	3.202	3.081	3.307	3.137	3.022	3.112	3.012	2.978	3.143	3.267	3.054	3.105	3.189	3.075	3.334
Cr	0.008	0.003	0.002	0.008	0.000	0.000	0.002	0.007	0.003	0.000	0.004	0.000	0.002	0.006	0.004
Mg	1.787	1.663	1.604	1.720	1.719	1.751	1.736	1.663	1.590	1.316	1.642	1.689	1.668	1.680	1.480
Ca	0.000	0.000	0.003	0.005	0.000	0.000	0.000	0.000	0.000	0.005	0.004	0.000	0.002	0.000	0.009
Mn	0.030	0.039	0.040	0.035	0.019	0.033	0.025	0.036	0.044	0.045	0.031	0.027	0.024	0.030	0.030
Fe	2.835	2.917	3.020	3.076	2.780	2.906	2.748	2.973	3.003	3.321	2.976	2.976	2.988	3.000	2.910
Ba	0.000	0.000	0.000	0.000	0.000	0.000	0.000	0.000	0.000	0.000	0.000	0.000	0.000	0.000	0.000
Na	0.039	0.027	0.020	0.025	0.024	0.041	0.028	0.019	0.035	0.019	0.028	0.040	0.014	0.010	0.050
K	1.832	1.867	1.870	1.747	1.847	1.829	1.852	1.841	1.855	1.862	1.822	1.819	1.802	1.870	1.780
Total	15.532	15.501	15.583	15.534	15.418	15.525	15.417	15.477	15.522	15.571	15.479	15.516	15.501	15.538	15.418

[a] Augen gneiss (type A), laminated augen gneiss (type B), mylonitic gneiss (type C)

Table 3 Bulk-rock compositions of orthogneisses (measured by XRF) representing different degrees of deformation. Oxides in wt%, trace elements in ppm

Sample	Augen gneiss (type A)							Laminated augen gneiss (type B)					Mylonitic gneiss (type C)							
	7	9	10	15	18	$\bar{x}$	2σ	13	19	22	$\bar{x}$	2σ	1	3	4	5	20	21	$\bar{x}$	2σ
SiO_2	72.14	69.52	70.61	69.78	71.25	70.66	1.08	71.51	69.82	70.40	70.58	1.22	69.73	70.30	69.70	69.10	70.63	69.95	69.90	0.47
Al_2O_3	14.53	14.24	14.92	14.35	14.76	14.56	0.29	15.69	14.45	14.63	14.93	0.95	14.77	14.59	14.92	14.60	15.03	14.92	14.81	0.17
Fe_2O_3	1.64	2.64	2.30	2.61	2.51	2.34	0.42	2.28	2.47	2.65	2.46	0.26	2.51	2.58	2.58	2.65	2.67	2.54	2.59	0.05
MnO	0.02	0.03	0.03	0.04	0.03	0.03	0.01	0.02	0.03	0.03	0.03	0.01	0.03	0.03	0.03	0.04	0.03	0.02	0.03	0.01
MgO	0.38	0.67	0.60	0.73	0.66	0.61	0.14	0.58	0.57	0.66	0.60	0.06	0.62	0.67	0.63	0.67	0.74	0.63	0.66	0.04
CaO	1.51	1.94	1.07	1.98	1.10	1.52	0.44	0.93	1.79	1.81	1.51	0.71	1.51	1.83	2.05	2.49	1.94	1.91	1.95	0.29
Na_2O	3.40	3.62	3.08	3.73	2.81	3.33	0.39	2.98	3.33	3.48	3.26	0.36	3.58	3.32	3.45	3.94	3.04	3.28	3.43	0.28
K_2O	4.88	5.05	5.26	4.74	5.00	4.99	0.20	5.21	5.04	4.34	4.86	0.66	4.91	4.36	4.59	4.66	4.16	4.75	4.57	0.24
TiO_2	0.24	0.37	0.33	0.35	0.38	0.34	0.06	0.38	0.35	0.37	0.36	0.02	0.36	0.35	0.38	0.39	0.41	0.35	0.37	0.02
P_2O_5	0.17	0.19	0.25	0.22	0.16	0.20	0.04	0.23	0.17	0.53	0.31	0.27	0.18	0.16	0.20	0.19	0.16	0.20	0.18	0.01
LOI	0.32	0.48	0.50	0.47	0.57			0.66	0.38	0.37			0.40	0.40	0.51	0.33	0.48	0.40		
Total	99.22	98.77	98.95	99.00	99.24			100.5	98.41	99.26			98.61	98.60	99.03	99.07	99.29	98.95		
Nb	8	11	10	10	10	10	1	10	11	10	10	1	10	10	11	10	11	11	11	0.4
Rb	141	161	171	151	154	155	12	170	158	149	159	15	141	142	147	137	163	171	150	12
Sr	132	115	109	134	92	116	17	106	123	126	118	16	160	125	126	155	165	112	141	20
V	22	31	27	32	34	29	5	35	37	32	35	4	23	31	36	31	33	35	31	4
Y	32	25	21	36	21	27	7	32	33	40	35	6	31	33	45	48	43	33	39	7
Zr	126	158	137	153	159	146	15	150	151	147	149	3	143	155	159	156	163	152	155	6
A/CNK	1.07	0.95	1.18	0.97	1.22			1.28	1.02	1.07			1.06	1.08	1.04	0.91	1.15	1.06		
NK/A	0.75	0.80	0.72	0.79	0.68			0.67	0.76	0.71			0.76	0.70	0.71	0.79	0.63	0.70		

Fourteen whole-rock samples were analysed for major and selected trace elements with a Siemens SRS X-ray fluorescence (XRF) spectrometer at the Institut für Mineralogie, Universität Münster (Table 3). The rare earth elements were analysed by an ICP-MS at Activation Laboratories Ltd., Ancaster, Ontario, using a lithium metaborate/lithium tetraborate fusion followed by acid digestion (Table 4).

Table 4 Rare earth element analyses (measured by ICP-MS) of samples representing the three textural variants. All concentrations are given in ppm

Type[a]	Sample	La	Ce	Pr	Nd	Sm	Eu	Gd	Tb	Dy	Ho	Er	Tm	Yb	Lu
A	7	20.8	44.3	5.02	19.4	4.50	0.97	4.76	0.87	5.59	1.21	3.75	0.52	3.24	0.47
A	10	6.98	–	2.11	8.41	2.35	0.51	2.55	0.56	3.95	0.91	2.93	0.45	2.87	0.43
A	18	17.3	–	3.70	13.3	2.71	0.42	2.65	0.51	3.42	0.79	2.60	0.41	2.73	0.41
B	22	27.5	64.7	6.97	27.4	6.03	0.91	5.90	1.10	7.12	1.50	4.54	0.64	3.79	0.56
C	3	19.5	55.9	5.16	19.8	4.54	0.73	4.51	0.84	5.71	1.25	3.87	0.56	3.46	0.50
C	20	30.4	70.0	7.94	30.4	7.02	1.03	6.81	1.28	7.85	1.62	4.81	0.67	3.95	0.56

[a] Augen gneiss (type A), laminated augen gneiss (type B), mylonitic gneiss (type C)

Table 5 Rb–Sr isotopic data of orthogneisses representing textural types A, B and C

Type[a]	Sample		Grain size (μm)	Rb (ppm)	Sr (ppm)	$^{87}Rb/^{86}Sr$	$^{87}Sr/^{86}Sr$
A	7	Whole rock		140.5	134.2	3.034	0.72916(2)
		Whole rock[b]					0.72913(1)
		Phengite	250–180	423.8	14.39	88.85	1.14155(4)
		Phengite[b]	180–125	421.7	13.96	91.19	1.1533(2)
		Biotite	250–180	767.4	4.512	622.5	3.4168(1)
		Biotite[b]	180–125	751.9	7.036	355.1	2.22491(8)
		Biotite[b]	125–63	723.2	10.82	210.3	1.5957(6)
A	10	Whole rock		167.2	113.1	4.289	0.73565(2)
		Whole rock[b]					0.73567(2)
		Phengite	250–180	410.3	12.33	100.9	1.19701(4)
		Phengite[b]	180–125	414.4	10.73	117.9	1.2750(1)
		Biotite	250–180	731.1	2.853	1118	5.9145(2)
		Biotite[b]	180–125	713.6	3.915	686.3	3.7884(4)
A	18	Whole rock		153.1	99.40	4.468	0.73605(2)
		Phengite	250–180	412.4	15.91	77.81	1.08915(3)
		Biotite	250–180	675.1	2.463	1259	6.7230(3)
B	22	Whole rock		144.2	125.3	3.336	0.73172(2)
		Phengite	250–180	442.5	16.14	82.44	1.11028(4)
		Biotite	250–180	758.4	4.277	673.0	3.8941(1)
C	3	Whole rock		136.7	126.6	3.131	0.72952(2)
		Whole rock[b]					0.72946(1)
		Phengite	250–180	405.9	31.58	37.88	0.89772(3)
		Phengite[b]	180–125	402.2	27.64	42.99	0.92152(8)
		Biotite	250–180	674.7	9.843	218.3	1.73755(4)
		Biotite[b]	180–125	681.0	7.675	290.3	2.04288(4)
		Biotite[b]	125–63	633.3	16.07	120.3	1.2708(1)
C	20	Whole rock		150.9	157.7	2.774	0.72767(3)
		Phengite	250–180	417.0	22.27	55.62	0.98241(4)
		Biotite	250–180	722.3	10.22	226.1	1.78370(4)

[a] Augen gneiss (type A), laminated augen gneiss (type B), mylonitic gneiss (type C)

[b] Sr was loaded with TaF_5 on W filaments; in all other cases, Sr was loaded with H_3PO_4 on Ta filaments

Whole-rock powders were prepared by standard techniques from carefully cleaned samples (3–7 kg) using a jaw crusher and a tungsten carbide mill. For separation of white mica and biotite, some of the crushed material was reduced in size by grinding for a few seconds in a tungsten carbide mill. Fines were removed by sieving and mica was enriched by standard techniques (Frantz magnetic separator, adherence to a piece of paper). After hand picking the mica packages under a stereomicroscope, possible contaminants located between individual sheets and at their rims were removed by grinding under ethanol in an agate mortar. Mica concentrates (optically pure >99%) were then washed in ethanol (p.a.) and H_2O (three times distilled) in an ultrasonic bath. For Rb–Sr analyses, whole-rock powders (about 100 mg) and mineral separates (ca. 30 mg) were mixed with a ^{87}Rb–^{84}Sr spike in Teflon screw-top vials and dissolved in a HF–HNO_3 (5:1) mixture on a hot plate. After drying, 6 N HCl was added to the residue. This mixture was homogenized on a hot plate. After a second evaporation to dryness, Rb and Sr were separated by standard ion-exchange procedures (AG 50W-X8 resin) on quartz glass columns using 2.5 and 6 N HCl as eluents. For mass-spectrometric analysis, Rb was loaded on Ta filaments (double filament) with H_2O. For Sr analysis (single filament), a first sample series was loaded on Ta filaments with H_3PO_4. A second series was analysed using TaF_5 on W filaments. Isotope analyses were carried out at the Zentrallaboratorium für Geochronologie at the Institut für Mineralogie, Universität Münster using a VG

Table 6 Rb–Sr phengite–whole-rock and biotite–whole-rock ages of orthogneisses representing textural types A, B and C

Type[a]	Sample		Grain size (μm)	Ma±2σ
A	7	Phengite	250–180	337.6±7.0
		Phengite	180–125	338.1±7.0
		Biotite	250–180	304.9±6.2
		Biotite	180–125	298.6±6.0
		Biotite	125–63	293.9±6.0
A	10	Phengite	250–180	335.5±7.0
		Phengite	180–125	333.5±7.0
		Biotite	250–180	326.4±6.6
		Biotite	180–125	314.5±6.4
A	18	Phengite	250–180	338.2±7.2
		Biotite	250–180	335.1±6.8
B	22	Phengite	250–180	336.6±7.2
		Biotite	250–180	331.8±6.6
C	3	Phengite	250–180	340.1±7.4
		Phengite	180–125	338.5±7.4
		Biotite	250–180	329.1±6.6
		Biotite	180–125	321.4±6.6
		Biotite	125–63	324.7±6.6
C	20	Phengite	250–180	338.6±7.2
		Biotite	250–180	332.3±6.8

[a] Augen gneiss (type A), laminated augen gneiss (type B), mylonitic gneiss (type C)

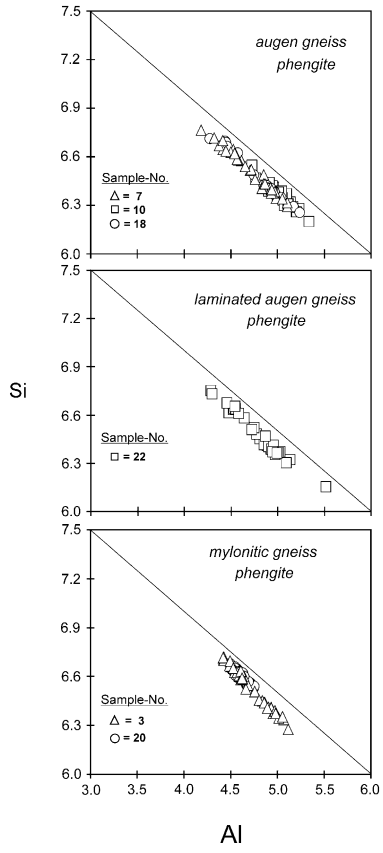

Fig. 4 Si vs. Al diagram for phengite. *Type A* Augen gneiss; *type B* laminated augen gneiss; *type C* mylonitic gneiss. The *reference line* indicates substitution along the aluminoceladonite–muscovite join

Sector 54 multicollector mass spectrometer (Sr) and a NBS-type Teledyne mass spectrometer (Rb). Correction for mass fractionation is based on a $^{86}Sr/^{88}Sr$ ratio of 0.1194. Rb ratios were corrected for mass fractionation using a factor deduced from multiple measurements of Rb standard NBS 607. Total procedural blanks were less than 0.1 ng for Rb and 0.15 ng for Sr. Based on repeated measurements, the $^{87}Rb/^{86}Sr$ ratios were assigned an uncertainty of 1% (2σ). For the $^{87}Sr/^{86}Sr$ isotope ratio uncertainties represent the within-run statistics (2σ). Repeated measurements of standard NBS 987 gave an average $^{87}Sr/^{86}Sr$ ratio of 0.710281±16 (2σ, *n*=23). All ages and element concentrations were calculated using the constants recommended by the IUGS (Steiger and Jäger 1977). Rb–Sr ages were calculated using the least squares regression technique of York (1969). Ages and errors are reported at the 2σ level. The Rb–Sr isotopic data are summarized in Tables 5 and 6.

Results

Mica compositions

Six samples were analysed with the electron microprobe. For each sample, the composition of 30–40 white micas and 30–40 biotites were determined. All white micas are phengites that show the same range in Si (6.2–6.8 per formula unit, based on 22 oxygens; Fig. 4; Table 1). It is not possible to decide whether this compositional feature reflects zoning of individual grains or indicates microstructurally different grains. The mineral chemistry of biotite from the different orthogneisses is indistinguishable (Fig. 5; Table 2). Biotite has Fe/(Fe+Mg) ratios between 0.5 and 0.8. TiO_2 concentrations are highly variable and range from 2.18 to 3.80.

Whole-rock geochemistry

In order to evaluate deformation-related chemical changes, bulk-rock compositions of mylonitic gneisses and less deformed precursors were determined for 14 samples, representing the three textural variants. Analytical results are summarized in Tables 3 and 4 and shown in Fig. 6. All samples are compositionally homogeneous, independent of the degree of deformation (Tables 3 and 4, Fig. 6). The distribution of rare earth elements shows consistent patterns for orthogneisses of different textural types, although deformation apparently caused a trend towards higher concentrations (Fig. 6). Bulk-rock compositions and the CIPW-norms indicate granitic protoliths. In the normative An–Ab–Or diagram of Barker (1979, not shown), the studied samples plot into the granite and quartz monzonite field. Streckeisen's diagram (1974; Fig. 7) indicates monzogranitic precursors.

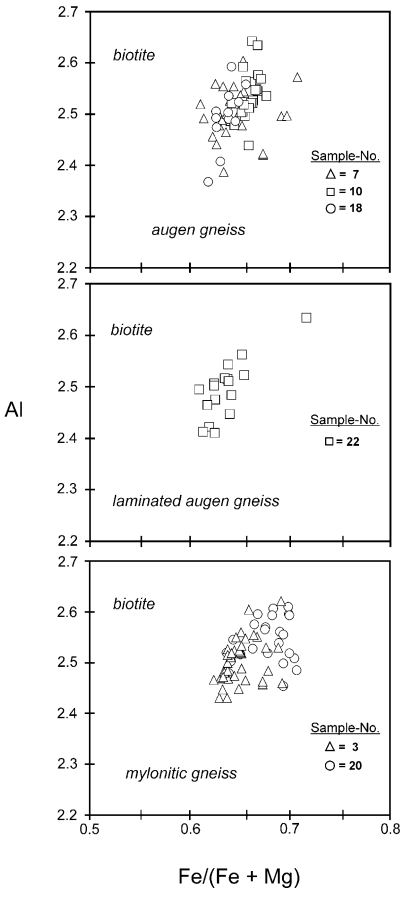

Fig. 5 Al vs. Fe/(Fe+Mg) diagram for biotite. *Type A* Augen gneiss; *type B* laminated augen gneiss; *type C* mylonitic gneiss

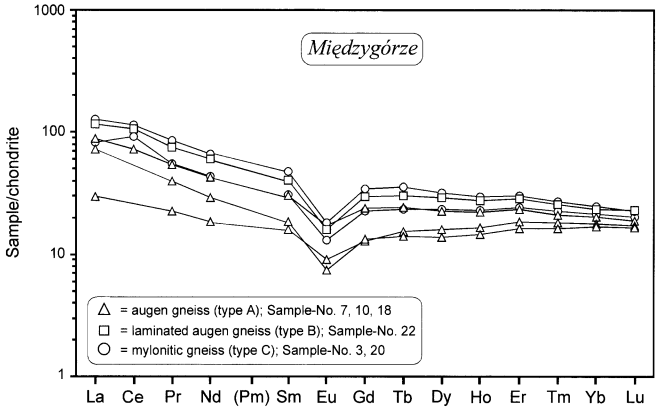

Fig. 6 Chondrite-normalized REE patterns for orthogneisses from the Śnieżnik Mountains. Chondritic values from McDonough and Sun (1995)

Most samples are peraluminous with A/CNK ratios between 1.06 and 1.28. Three samples, representing textural variants A and C, show metaluminous characteristics with A/CNK ratios between 0.91 and 0.97, and NK/A between 0.79 and 0.80.

In order to identify element losses and gains associated with the development of shear zones, possible changes in mass or volume must be taken into consideration (Gresens 1967). A mathematical solution to evaluate composition/volume relationships was presented by Gresens (1967) and transformed into a simplified graphical method by Grant (1986). In Grant's diagram element losses and gains are indicated by deviation from a line of equal concentration, which is termed an isocon.

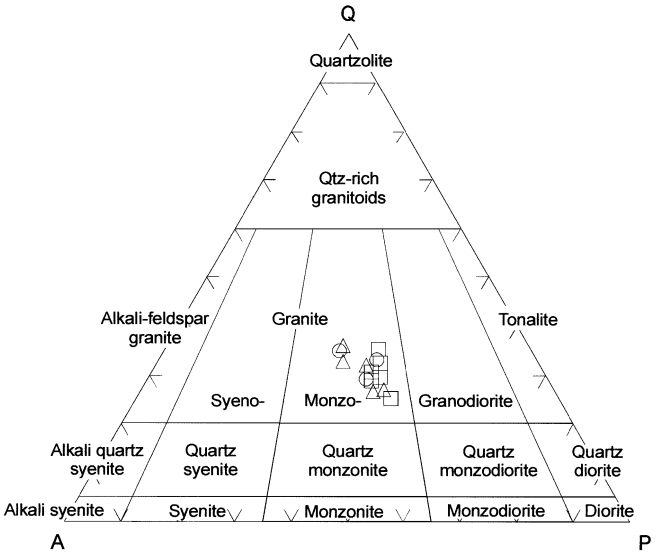

Fig. 7 CIPW normative Q–A–P ternary diagram according to Streckeisen (1974) indicating granitic precursors for orthogneisses of different textural types (*triangle* augen gneiss, type A; *circle* laminated augen gneiss, type B; *square* mylonitic gneiss, type C)

As shown in Fig. 8, progressive stages of shearing are not associated with significant compositional changes of major and most trace elements. Within error (±2σ) data points for most elements overlap with the 1:1 reference isocon, indicating almost mass conservative shearing (note that the rock densities do not differ between the three textural variants). Minor differences (e.g. Y and V) are interpreted to represent original heterogeneities of the protoliths.

Rb–Sr geochronology

For Rb–Sr studies, six samples were selected. The isotopic results and ages are listed in Tables 5 and 6.

The Rb concentrations of phengite and biotite range from 402 to 443 ppm and from 633 to 767 ppm, respectively. The Sr concentrations vary between 10.7 and 31.6 ppm in phengite and between 2.5 and 16.1 ppm in biotite. The Rb concentrations of the whole rocks range from 137 to 167 ppm, those of Sr from 99 to 158 ppm. The initial $^{87}Sr/^{86}Sr$ ratios define a narrow range between 0.7144 and 0.7160. For all samples and grain-size fractions, Rb–Sr phengite–whole-rock dating yielded ages between 340 and 334 Ma (Tables 5 and 6, Fig. 9). The weighted mean age of two point isochrons is 337.4±2.3 Ma (n=9). In contrast Rb–Sr biotite–whole-rock ages show a larger variability and range from 335 to

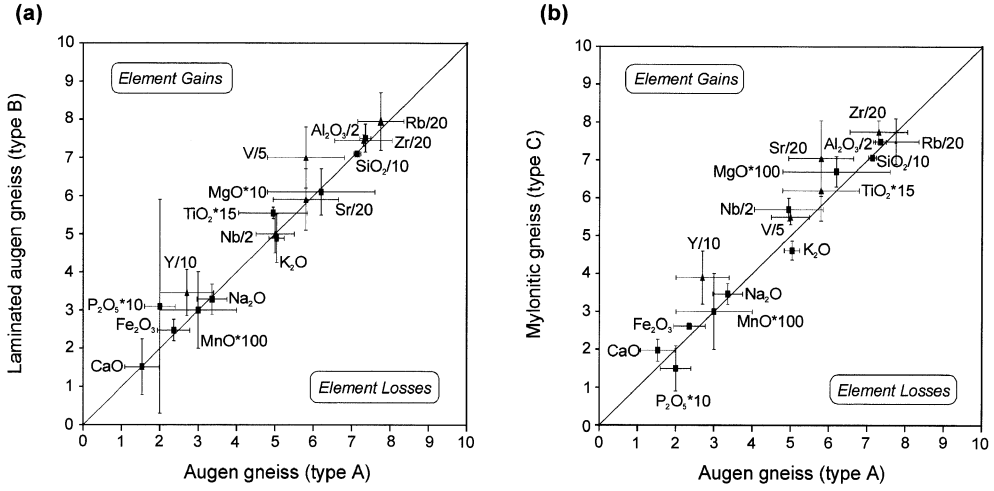

Fig. 8 Isocon diagram after Grant (1986) using average bulk rock compositions of **a** augen gneiss vs. laminated augen gneiss and **b** augen gneiss vs. mylonitic gneiss. Oxides in wt%, trace elements in ppm. Concentrations are scaled to fit on the plot. *Reference line* indicates the constant mass isocon

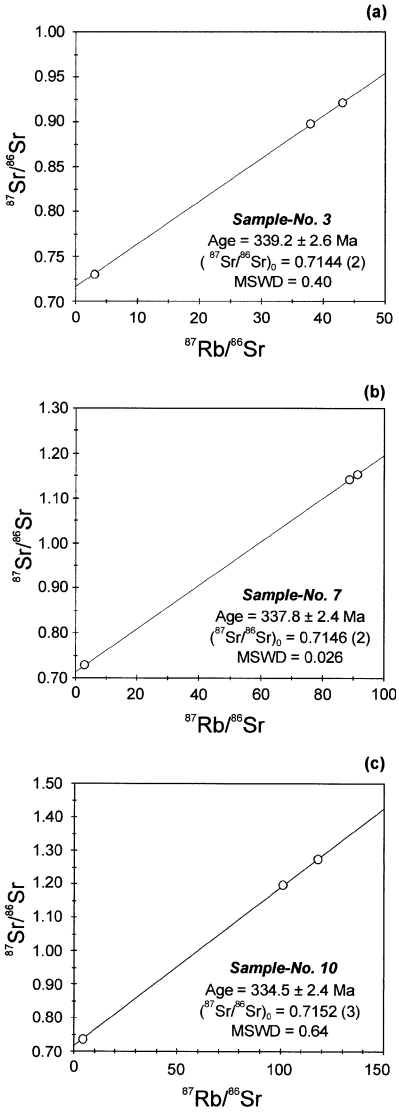

Fig. 9 Rb–Sr isochron diagrams of orthogneiss samples; *a*, *b* and *c* internal mineral isochrons based on phengite and whole-rock isotopic data

294 Ma (Tables 5 and 6). Seven biotite–whole-rock pairs provide ages between 335 and 321 Ma (weighted mean age: 328.6±4.4 Ma, Tables 5 and 6). However, three size fractions of sample 7 yielded significantly younger ages (weighted mean age: 299±14 Ma); one biotite fraction of sample 10 provided an age of 314.5±6.4 Ma (Tables 5 and 6). In samples 7 and 10, the biotite ages seem to be correlated with the grain-size. The smallest analysed grain-size fractions yielded younger ages. Because of the more heterogeneous Rb–Sr isotope characteristics of the biotites, internal mineral-whole-rock isochrons (not shown) were characterized by high MSWD values and dates with large uncertainties, which are of doubtful geological significance.

Discussion and conclusions

The heterogeneous deformation of the Śnieżnik augen gneisses caused the transformation to different textural types. Highly deformed rocks occur in small-scale shear zones (centimetre- to metre-scale) that developed during amphibolite-facies metamorphism.

Bulk rock-compositions of variably deformed orthogneisses are not different and yield no indications for significant deformation-enhanced element mobility and redistribution. Thus, metasomatic alteration, as a result of channelized fluid fluxes in the shear zones, can largely be ruled out. If at all, only very limited fluid–rock interaction took place. This interpretation is in agreement with the observation that local in-situ partial melting is restricted to small domains within the studied shear zone, suggesting differences in the availability of fluids. Minor compositional differences between the three textural types of gneisses are interpreted to represent the primary heterogeneity of the protoliths. Geochemical changes associated with ductile deformation were not recognized.

Independent of the degree of deformation, the phengite and biotite populations of the different gneiss variet-

ies are compositionally similar. However, intrasample phengite compositions disclose a complex recrystallization history. The Si-values of phengites range from 6.2 to 6.8, indicating a large range in pressures (Massonne and Schreyer 1987). This variability either suggests that different phengite generations occur, or that individual grains are strongly zoned. Thus, phengite compositions record a polystage history under different pressure conditions. It is not known whether this feature developed on the prograde or retrograde path. However, a late formation of the low-Si phengites is considered to be more realistic than the preservation of phengite that is associated with early stages of the metamorphic history. In any case, mixing of different mica generations or the presence of compositionally complex micas, possibly with an inherited component, may cause problems to constrain the age for a distinct event precisely, when multigrain dating is applied. Multigrain dating of such populations will only provide an upper time limit for the last overprint or a lower time limit for an older event (e.g. Bröcker and Franz 2000).

Field observations indicate that the mylonitic gneisses were affected locally by a late syn- or post kinematic migmatization. As a consequence, the deformation event is not directly dated by the Rb–Sr method because phengite and biotite apparently recrystallized above their commonly assumed closure temperatures (500±50 and 300±50 °C, respectively; e.g. Jäger 1979; Mezger 1990). However, a record of the cooling history brackets the timing of migmatization and yields a minimum age for development of the ductile shear zone.

Phengite–whole-rock isochrons provide consistent Rb–Sr ages (340–334 Ma) that are independent both of grain-size and degree of deformation (weighted mean age: 337.4±2.3 Ma; *n*=9). Biotite–whole-rock data show a larger spread. Seven of 11 individual dates range between 335 and 321 Ma (weighted mean age: 328.6± 4.4 Ma). Four fractions are considerably younger (315–294 Ma), and the resulting age range between phengite dates and this group is too large to be only related to cooling. We consider retrograde disturbance because of superimposed alteration (late deformation or late fluid–rock interaction) as the most likely explanation. In any case, the age differences between the distinct Rb–Sr phengite and biotite age groups are interpreted to date cooling through their respective closure temperatures after a thermal peak in Variscan times. (It should be noted that the true cooling age difference between phengite and biotite is possibly reduced by a second phengite generation that contaminates the oldest phengite-population.)

The ages from this study are similar to previously reported metamorphic ages for gneisses (Rb–Sr phengite, biotite, Borkowska et al. 1990; $^{40}Ar/^{39}Ar$ hornblende, muscovite, biotite, Steltenpohl et al. 1993; U–Pb zircon, Turniak et al. 2000), eclogites and granulites (Sm–Nd garnet-clinopyroxene–whole-rock, Brueckner et al. 1991; Klemd and Bröcker 1999) from the Orlica-Śnieżnik dome. Isotopic systems with vastly different closure temperatures record similar ages of 330 to 340 Ma (Brueckner et al. 1991; Steltenpohl et al. 1993; Klemd and Bröcker 1999; Turniak et al. 2000). These apparently simple geochronological results contrast with petrographical and structural observations (e.g. Don et al. 1990 and references therein) that indicate a complex geological evolution for the Orlica-Śnieżnik dome. At present, the coincidence of ages is best explained by assuming very high cooling rates that must have been in excess of 50 °C/Ma from the time of peak metamorphism (T_{max} ~700 °C) to the closure of the Rb–Sr system in phengite (ca. 500 °C). A comparison of the Rb–Sr biotite with the phengite ages from the Orlica-Śnieżnik dome (Tables 5 and 6) indicates a difference in the time of closure of 8.8±6.7 Ma. Because the difference of the closure temperature of Rb–Sr system in biotite and phengite is assumed to be ca. 200 °C, this corresponds to cooling rates of 13–87 °C/Ma for the temperature interval between 500 and 300 °C. Such rapid cooling rates cannot be a result of erosional uplift following an orogenic cycle, but are more characteristic of fast tectonic uplift associated with orogenic collapse. High cooling rates are also compatible with the model of tectonic overthrusting suggested for the study area by Turniak et al. (2000). However, field relations and textural features combined with thermochronological constraints indicate that the studied mylonite zone is not an extensional shear zone. The static recrystallization of the mylonite fabric and the local migmatitic overprint clearly indicate that shearing is a pre- or synmetamorphic feature, relative to the T_{max} stage (~700 °C). Thus, we conclude that the shearing was not active after the orogenic compressional phase. An interesting, yet unsolved issue is the question whether these shear zones are of importance for the tectonic incorporation of eclogites that are found in close spatial association to the sample location.

In the present case, Rb–Sr mica chronology cannot successfully be applied for direct dating of deformation because mylonitization occurred at temperatures significantly above the Rb–Sr closure temperatures for phengite and biotite. The Rb–Sr ages constrain a minimum age of 340 Ma for the final thermal event and the development of the deformational fabric. However, the new data do not reveal more detailed information about the temporal relation between deformation and metamorphism, namely whether the ductile deformation and the peak-temperature stage represent a more or less continuous process of short duration, or are significantly separated in time (e.g. Caledonian versus Variscan or Early versus Late Variscan events). The importance of a possible Caledonian tectono-metamorphic history remains unclear. The very rapid cooling has caused a situation where different isotope systems provide overlapping ages for different segments of the P–T-deformation path, thus preventing a clear temporal resolution of distinct stages in the evolution of the Orlica-Śnieżnik dome. However, the combined age constraints currently available indicate that the last peak metamorphic conditions must have been reached shortly before 340 Ma. Thus, this study further documents the importance of Variscan metamor-

phism in the West Sudetes. The new Rb–Sr mica isochron ages not only provide constraints for the late stages of the Variscan orogeny, but closely approximate the timing for the latest HT-metamorphic climax and yield important constraints on the early post-peak metamorphic thermal history.

Acknowledgements Thanks are due to H. Baier for laboratory assistance and to S. Rochnowski for support on the mass spectrometer. Careful reviews by A. Cliff (Leeds), K. Hammerschmidt (Berlin), D. Marheine (Montpellier), U. Poller (Mainz) and J. Zeck (Copenhagen) helped to improve the manuscript. Financial support of the Deutsche Forschungsgemeinschaft to the Zentrallaboratorium für Geochronologie (Münster) is greatly acknowledged.

References

Bakun-Czubarow N (1968) Geochemical characteristics of eclogites from the environs of Nowa Wieś in the region of Śnieżnik Kłodzki. Arch Mineral 28:244–371

Bakun-Czubarow N (1991a) On the possibility of quartz pseudomorphs after coesite in the eclogite–granulite rock series of the Złote Mountains in the Sudetes (SW Poland). Arch Mineral 42:5–16

Bakun-Czubarow N (1991b) Geodynamic significance of the Variscan HP eclogite–granulite series of the Złoty Mountains in the Sudetes. Publ Inst Geophys Pol Acad Sci A-19 (236):215–242

Barker F (1979) Trondhjemite: definition, environment and hypotheses of origin. In: Barker F (ed) Trondhjemites, dacites and related rocks. Elsevier, Amsterdam, pp 1–12

Borkowska M, Dörr W (1998) Some remarks on the age and mineral chemistry of orthogneisses from the Lądek-Śnieżnik Metamorphic Massif – Sudetes, Poland. Terra Nostra 98(2):27–30

Borkowska M, Orlowski R (1999) Orthogneisses of the Lądek-Śnieżnik metamorphic complex (Sudetes, Poland): their mineral chemistry and age relations. Terra Nostra 99(1):62–63

Borkowska M, Choukroune P, Hameurt F, Martineau F (1990) A geochemical investigation of the age, significance and structural evolution of the Caledonian-Variscan granite–gneisses of the Śnieżnik metamorphic area, central Sudetes, Poland. Geol Sudetica 25:1–27

Bröcker M, Franz L (2000) Contact metamorphism on Tinos (Cyclades, Greece): the importance of tourmaline, timing of the thermal overprint and Sr isotope characteristics. Mineral Petrol 70:257–283

Bröcker M, Klemd R (1996) Ultrahigh-pressure metamorphism in the Śnieżnik Mountains (Sudetes, Poland): P–T constraints and geological implications. J Geol 104:417–433

Brueckner HK, Medaris LG Jr, Bakun-Czubarow N (1991) Nd and Sr age and isotope patterns from Variscan eclogites of the eastern Bohemian Massif. Neues Jahrb Mineral Abh 163:169–196

Cymerman Z, Piasecki MAJ, Seston R (1997) Terranes and terrane boundaries in the Sudetes, northeast Bohemian Massif. Geol Mag 134:717–725

Don J (1977) The new data on interrelations between Śnieżnik and Gierałtów gneisses (Sudetes). Estudios Geol 33:182–192

Don J (1982a) Die Entwicklung der Migmatite in der Zone der Übergangsgneise von Międzygórze (Metamorphikum des Śnieżnik – Sudety). In: Deformation und Metamorphose von Gesteinen II. Veröffentlichungen des Zentralinstituts für Physik der Erde, Akademie der Wissenschaften der DDR, Nr. 72:5–20

Don J (1982b) The Sienna synform and the relationship of gneisses to the deformational stages distinguished in the Śnieżnik metamorphic massif (Sudetes). Geol Sudetica 17:103–124

Don J (1989) On the position of the eclogites within the gneisses of Międzygórze (Śnieżnik metamorphic massif – Sudetes). In: Indicators of structural evolution in polyphase deformed metamorphic complexes. Polish Academy of Sciences and Institute of Geological Sciences, Wrocław University, pp 44–58

Don J (2001) The transitional border zone between the Śnieżnik augen gneisses and the Gierałtów migmatites within the Międzygórze anticlinorium. Mineral Soc Poland Spec Pap 19:203–205

Don J, Dumicz M, Wojciechowska I, Żelaźniewicz A (1990) Lithology and tectonics of the Orlica-Śnieżnik Dome, Sudetes – recent state of knowledge. Neues Jahrb Geol Paläontolo Abh 179:159–188

Dumicz M (1979) Tectonogenesis of the metamorphosed series of the Kłodzko district: a tentative explanation. Geol Sudetica 14:29–46

Dumicz M (1988) Złoty Stok-Skrzynka structural element in the light of mesostructural analysis of Lądek-Śnieżnik metamorphic terrain. Geol Sudetica 23:92–106

Fossen H, Dallmeyer RD (1998) $^{40}Ar/^{39}Ar$ muscovite dates from the nappe region of southwestern Norway: dating extensional deformation in the Scandinavian Caledonides. Tectonophysics 285:119–133

Freeman SR, Inger S, Butler RWH, Cliff RA (1997) Dating deformation using Rb–Sr in white mica: greenschist facies deformation ages from the Entrelor shear zone, Italian Alps. Tectonics 16:57–76

Freeman SR, Butler RWH, Cliff RA, Rex DC (1998a) Direct dating of mylonite evolution: a multi-disciplinary geochronological study from the Moine thrust zone, NW Scotland. J Geol Soc Lond 155:745–758

Freeman SR, Butler RWH, Cliff RH, Inger S, Barnicoat TAC (1998b) Deformation migration in an orogen-scale shear zone array: an example from the basal Brianconnais thrust, internal Franco-Italian Alps. Geol Mag 135:349–367

Getty S, Gromet P (1992) Geochronological constraints on ductile deformation, crustal extension, and doming about a basement-cover boundary, New England Appalachians. Am J Sci 292:359–397

Grant JA (1986) The isocon diagram – a simple solution to Gresens' equation for metasomatic alteration. Economic Geol 81:1976–1982

Gresens RL (1967) Composition–volume relationships of metasomatism. Chem Geol 2:47–65

Gromet P (1991) Direct dating of deformational fabrics. Mineral Assoc Can 19:167–189

Jäger E (1979) The Rb–Sr method. In: Jäger E, Hunziker JC (eds) Lectures in isotope geology. Springer, Berlin Heidelberg New York, pp 13–26

Klemd R, Bröcker M (1999) Fluid influence on mineral reactions in ultrahigh-pressure granulites: a case study in the Śnieżnik Mts. (West Sudetes, Poland). Contrib Mineral Petrol 136:358–373

Klemd R, Bröcker M, Schramm J (1995) Characterization of amphibolite-facies fluids of Variscan eclogites from the Orlica-Śnieżnik dome (Sudetes, SW Poland). Chem Geol 119:101–113

Kröner A, Jaeckel P, Hegner E, Opletal M (2001) Single zircon ages and whole-rock Nd isotopic systematics of early Palaeozoic granitoid gneisses from the Czech and Polish Sudetes (Jizerske hory, Krkonose Mountains and Orlice-Sneznik Complex). Int J Earth Sci (Geol Rundsch) 90:304–324

Kryza R, Pin C, Vielzeuf D (1996) High pressure granulites from the Sudetes (south-west Poland): evidence of crustal subduction and collisional thickening in the Variscan Belt. J Metamorph Geol 14:531–546

Massonne H-J, Schreyer W (1987) Phengite geobarometry based on the limiting assemblage with K-feldspar, phlogopite, and quartz. Contrib Mineral Petrol 96:212–224

Mazur S, Aleksandrowski P (2001) The Tepla(?)/Saxothuringian suture in the Karkonosze-Izera massif, western Sudetes, central European Variscides. Int J Earth Sci (Geol Rundsch) 90:341–360

McDonough WF, Sun S-S (1995) The composition of the Earth. Chem Geol 120:223–253

Mezger K (1990) Geochronology in granulites. In: Vielzeuf D, Vidal P (eds) Granulites and crustal evolution. NATO Advanced Study Institute Series 311, pp 451–470

Oliver GJH, Corfu F, Krogh TE (1993) U–Pb ages from SW Poland: evidence for a Caledonian suture zone between Baltica and Gondwana. J Geol Soc Lond 150:355–369

Prikryl R, Schulmann K, Melka R (1996) Perpendicular fabrics in the Orlicke hory orthogneisses (western part of the Orlice-Sneznik Dome, Bohemian Massif) due to high temperature E–W deformational event and late lower temperature N–S overprint. J Czech Geol Soc 41:156–166

Scheuber E, Hammerschmidt K, Friedrichsen H (1995) $^{40}Ar/^{39}Ar$ and Rb–Sr analysis from ductile shear zones from the Atacama Fault Zone, northern Chile: the age of deformation. Tectonophysics 250:61–87

Smulikowski K (1967) Eclogites of the Śnieżnik Mts. In the Sudetes. Geol Sudetica 3:7-180

Steiger RH, Jäger E (1977) Subcommission on geochronology: convention on the use of decay constants in geo- and cosmochronology. Earth Planet Sci Lett 36:359–362

Steltenpohl MG, Cymerman Z, Krogh EJ, Kunk MJ (1993) Exhumation of eclogitized continental basement during Variscan lithospheric delamination and gravitational collapse, Sudety Mountains, Poland. Geology 21:1111–1114

Streckeisen A (1974) Classification and nomenclature of plutonic rocks. Geol Rundsch 63:773–786

Turniak K, Mazur S, Wysoczański R (2000) SHRIMP zircon geochronology and geochemistry of the Orlica-Śnieżnik gneisses (Variscan belt of Central Europe) and their tectonic implications. Geodinam Acta 13:293–312

van Breemen O, Aftalion M, Bowes DR, Dudek A, Misar Z, Povondra P, Vrana S (1982) Geochronological studies of the Bohemian Massif, Czechoslovakia, and their significance in the evolution of Central Europe. Trans R Soc Edinb Earth Sci 73:89–108

York D (1969) Least squares fitting of a straight line with correlated errors. Earth Planet Sci Lett 5:320–324

Żelaźniewicz A (1984) Synmetamorphic penetrative mylonitization in orthogneisses of the Bystrzyca Mts, Sudetes. Acta Geol Polonica 34:111–135

Żelaźniewicz A (1988) Orthogneisses due to irrotational extension, a case from the Sudetes, Bohemian Massif. Geol Rundsch 77:671–682